

# Microscopy-based high-throughput assays enable multi-parametric analysis to assess adverse effects of nanomaterials in various cell lines

Iris Hansjosten<sup>1</sup> · Juliane Rapp<sup>1</sup> · Luisa Reiner<sup>1</sup> · Ruben Vatter<sup>1</sup> · Susanne Fritsch-Decker<sup>1</sup> · Ravindra Peravali<sup>1</sup> · Taina Palosaari<sup>2</sup> · Elisabeth Joossens<sup>2</sup> · Kirsten Gerloff<sup>2</sup> · Peter Macko<sup>2</sup> · Maurice Whelan<sup>2</sup> · Douglas Gilliland<sup>2</sup> · Isaac Ojea-Jimenez<sup>2</sup> · Marco P. Monopoli<sup>3</sup> · Louise Rocks<sup>3</sup> · David Garry<sup>3</sup> · Kenneth Dawson<sup>3</sup> · Peter J. F. Röttgermann<sup>4</sup> · Alexandra Murschhauser<sup>4</sup> · Joachim O. Rädler<sup>4</sup> · Selina V. Y. Tang<sup>5</sup> · Pete Gooden<sup>5</sup> · Marie-France A. Belinga-Desaunay<sup>6</sup> · Abdullah O. Khan<sup>6</sup> · Sophie Briffa<sup>6</sup> · Emily Guggenheim<sup>6</sup> · Anastasios Papadimitris<sup>6</sup> · Iseult Lynch<sup>6</sup> · Eugenia Valsami-Jones<sup>6</sup> · Silvia Diabaté<sup>1</sup> · Carsten Weiss<sup>1</sup>

Received: 21 April 2017 / Accepted: 25 October 2017 / Published online: 8 November 2017  
© Springer-Verlag GmbH Germany 2017

**Abstract** Manufactured nanomaterials (MNMs) selected from a library of over 120 different MNMs with varied compositions, sizes, and surface coatings were tested by four different laboratories for toxicity by high-throughput/-content (HT/C) techniques. The selected particles comprise 14 MNMs composed of CeO<sub>2</sub>, Ag, TiO<sub>2</sub>, ZnO and SiO<sub>2</sub> with different coatings and surface characteristics at varying concentrations. The MNMs were tested in different mammalian cell lines at concentrations between 0.5 and 250 µg/mL to link physical–chemical properties to multiple adverse effects. The cell lines are derived from relevant organs such

as liver, lung, colon and the immune system. Endpoints such as viable cell count, cell membrane permeability, apoptotic cell death, mitochondrial membrane potential, lysosomal acidification and steatosis have been studied. Soluble MNMs, Ag and ZnO, were toxic in all cell types. TiO<sub>2</sub> and SiO<sub>2</sub> MNMs also triggered toxicity in some, but not all, cell types and the cell type-specific effects were influenced by the specific coating and surface modification. CeO<sub>2</sub> MNMs were nearly ineffective in our test systems. Differentiated liver cells appear to be most sensitive to MNMs, Whereas most of the investigated MNMs showed no acute toxicity, it became clear that some show adverse effects dependent on the assay and cell line. Hence, it is advised that future nanosafety studies utilise a multi-parametric approach such as HT/C screening to avoid missing signs of toxicity. Furthermore, some of the cell type-specific effects should be followed up in more detail and might also provide an incentive to address potential adverse effects in vivo in the relevant organ.

**Electronic supplementary material** The online version of this article (<https://doi.org/10.1007/s00204-017-2106-7>) contains supplementary material, which is available to authorized users.

✉ Carsten Weiss  
carsten.weiss@kit.edu

<sup>1</sup> Karlsruhe Institute of Technology (KIT), Institute of Toxicology and Genetics, Hermann-von-Helmholtz-Platz 1, 76344 Eggenstein-Leopoldshafen, Germany

<sup>2</sup> European Commission, Joint Research Centre (JRC), Via E. Fermi 2749, 21027 Ispra (VA), Italy

<sup>3</sup> Centre for BioNano Interactions (CBNI), School of Chemistry and Chemical Biology, University College Dublin (UCD), Belfield, Dublin 4, Ireland

<sup>4</sup> Faculty of Physics and Center for NanoScience (CeNS), Ludwig-Maximilians-Universität München (LMU), Geschwister-Scholl-Platz 1, 80539 Munich, Germany

<sup>5</sup> Promethean Particles Ltd, 1-3 Genesis Park, Midland Way, Nottingham NG7 3EF, UK

<sup>6</sup> School of Geography Earth and Environmental Sciences (GEES), University of Birmingham (UoB), Edgbaston, Birmingham B15 2TT, UK

**Keywords** Manufactured nanomaterials · Toxicity · High-throughput screening · Cell type specificity · Cell death · Adverse outcome pathways · Nanosafety

## Introduction

As a result of the diversity of manufactured nanomaterials (MNM) in terms of their physical–chemical features such as chemical composition, surface modification/charge and size, the number of materials to be tested to ensure safe and responsible innovation is steadily increasing. Between 500 and 2000 MNMs are expected to be placed on the EU market

at volumes of at least 1 tonne/year and are consequently affected by registration obligations under REACH legislation, leading to total costs of up to €600 million to be borne by industry, mostly (around 80%), micro companies or Small and Medium Enterprises (European commission 2013). For effective safety screening and hazard ranking of MNMs, it is necessary to speed up the testing by *in vitro* test systems which include microscopy-based high-throughput/-content (HT/C) methods (Nel et al. 2013; Delaval et al. 2017). Microscopy-based screening approaches not only reduce time and costs, but also circumvent misinterpretation of results obtained by some conventional toxicity tests, with which MNMs often interfere (e.g. by binding the colorimetric reporter molecules). They can also provide the basis for quantitative structure (property)–activity relationships (QS(P)ARs), allow identification of no-observed-adverse-effect levels (NOAELs), support the development of MNMs with improved safety, help to rapidly unravel toxicity or adverse outcome pathways (AOPs) of MNMs and refine, reduce or replace (3 Rs) animal experiments, all of which could have an impact on the decisions and approaches of regulatory authorities (Tralau et al. 2015). Indeed, the absence of extensive grouping and read-across approaches validated for MNMs is a critical factor in the cost estimate given above for REACH evaluation of MNMs, which is substantially reduced under the assumption of grouping read-across methods, although these are currently absent for MNMs (European commission 2013).

Cells cultured *in vitro* represent ideal high-throughput and ethically acceptable systems to assess toxicity. The cellular endpoints could be based on knowledge acquired from AOPs which are conceptual constructs that describe existing knowledge on the link between a molecular initiating event (MIE) and an adverse outcome. A sequential chain of causally linked events is portrayed at different levels of biological organisation (Horvat et al. 2017; Gerloff et al. 2017).

The cell models used in this study are representative of human organs known to interact with, or accumulate, MNMs (Fig. S1). The human alveolar lung epithelial cell line A549 and the human colonic epithelial cell line HCT116 were chosen as representative models derived from the major target organs lung and colon, respectively. Macrophages, as part of the immune system, are found in the lung and in all other organs. As a representative cell line, the murine cell line RAW264.7 was chosen. MNMs that reach the blood stream will pass through the liver as the central organ for metabolism including detoxification of xenobiotics. Liver cells are represented by differentiated human HepaRG and non-differentiated human HepG2 cells.

Upon systemic MNM exposure, the liver is one of the main target organs for their accumulation and thus a site susceptible to induction of adverse effects. Toxicity to the liver, such as cell death, inflammation and/or steatosis (infiltration

of liver cells with fat, associated with a disturbance of the metabolism) can be monitored. Human primary hepatocytes are the most recommended tools, especially as they are competent for Cytochrome P450 (CYP)-mediated metabolism (Godoy et al. 2013). However, the widespread use of primary hepatocytes is limited by the restricted availability of liver tissue, their early phenotypic changes and their limited lifespan. On the contrary, traditional human liver cell lines such as HepG2 often lack the necessary enzymes and proteins required for a normal response of the liver to toxic triggers. The human hepatoma cell line HepaRG displays hepatocyte-like functions and expresses drug detoxifying enzymes at relatively high levels compared to cell lines such as HepG2 (Kanebratt and Andersson 2008). When plated at high density, they differentiate into hepatocyte-like cells which can be purified from the co-culture with biliary cells using selective trypsinisation. This method has successfully been used for high-throughput screening of chemicals (Cerec et al. 2007; Mennecozzi et al. 2012).

On the basis of previously developed AOPs, e.g. for determining chemically induced liver toxicity (Landesmann et al. 2012; Landesmann 2015), the development and use of potentially nano-specific AOPs are currently being discussed (Gerloff et al. 2017). This knowledge was used to carefully select endpoints for this study. The selected endpoints are either relevant events of general MNM-induced toxicity (general cytotoxicity, mitochondrial damage, and apoptosis) or cell type-specific adverse outcomes (i.e. liver-specific steatosis) that might be involved in MNM toxicity to the selected organ.

Cell death is not only one of the key events in general MNM toxicity but, more specifically, also might lead to the development of more complex pathologies such as fibrosis. Cell death can be determined by various markers. During apoptosis, cleaved caspase-3 can be found either in the cytoplasm or, at a later stage, also within the nucleus (Ramuz et al. 2003). These different localizations can be distinguished via HT/C screening to provide further insight into the stage (progression) of the apoptotic process. The shape and staining intensity of the nucleus, as, e.g. determined via Hoechst 33342 staining, further allows for a careful distinction between apoptosis and necrosis, as apoptosis leads to fragmentation of the nucleus, a decrease in its size and an increase in nuclear staining intensity, whereas nuclear swelling points towards a necrotic cell death. Additionally, Image-iT DEAD green or propidium iodide (PI) staining allows for the analysis of cells with a compromised cell membrane, which further indicates a necrotic or late apoptotic process, whereas the cell count provides information on the overall amount of cells which are still attached (either healthy or already in the apoptotic or necrotic state).

Mitochondria not only generate the cell's energy but also play a central role in the regulation of apoptosis and

calcium homeostasis. The maintenance of a negative mitochondrial membrane potential (MMP) is essential for normal adenosine triphosphate (ATP) production and is considered as a functional readout. Loss of MMP results in an imbalance of the energy status, and induces formation of reactive oxygen species (ROS), impairment of calcium homeostasis and the release of certain proteins. These processes are essential for the induction and execution of apoptosis (Kroemer et al. 2007).

Lysosomes play an important role in endocytotic, phagocytotic and autophagic processes in degrading cellular components or extracellular material (Stern et al. 2012). Lysosomal membrane integrity is vital to cellular functioning. Once the lysosomal membrane is ruptured (a process called lysosomal membrane permeabilization (LMP)), the lysosomal content is released into the cytosol which induces cell death (Yu et al. 2016).

Steatosis belongs to the wide range of non-alcoholic fatty liver diseases (NAFLDs) and is characterised by the accumulation of lipids within hepatocytes. Steatosis is a relatively mild symptom but can lead to the development of steatohepatitis, which is characterised by inflammatory cell recruitment, cirrhosis and ultimately development of hepatocellular carcinoma. Obese patients have a highly increased risk for the development of steatosis (Yoon and Cha 2014).

HT/C assays provide various parameters simultaneously, such as information on specific staining intensities and the exact staining localisation, shape of an organelle such as the nucleus and further parameters. These parameters enable conclusions to be drawn regarding the underlying mechanisms of toxicity of each MNM tested, and might allow for observation of the temporal development towards an adverse outcome.

Here, 14 metal and metal oxide MNMs as well as amine-modified polystyrene (PS-NH<sub>2</sub>) MNMs were selected due to their widespread industrial or commercial use, and as they are members of the OECD priority particle list (OECD 2010). Ceria (CeO<sub>2</sub>), titania (TiO<sub>2</sub>), zinc oxide (ZnO) and silver (Ag) MNMs display different redox activities and solubility and were used with different surface coatings. Silica MNMs were surface functionalized by either carboxylation or amino-modification to study the impact of surface charge on toxicity. As a positive control, PS-NH<sub>2</sub> MNMs were investigated, which have been shown previously to induce cell death in multiple cell types (e.g. HEK293, HepG2, hCMEC/D3, A549, SHSY5Y, 1321N1, RAW264.7) mostly by lysosomal damage (Anguissola et al. 2014; Xia et al. 2008).

The data generated by this work will not only be useful to analyse mechanisms of MNM toxicity but also provide the basis for establishment of QS(P)ARs, allow identification of NOAELs and guide follow-up studies in vivo.

## Materials and methods

### Nanomaterials

The MNMs used in this study are all from the NanoMILE project MNM library. More specifically, TiO<sub>2</sub> NM-103, TiO<sub>2</sub> NM-104, CeO<sub>2</sub> NM-212, ZnO NM-110, ZnO NM-111, and Ag NM-300 K MNMs were provided by the JRC (Joint Research Centre, Ispra, Italy) repository and were described previously (Rasmussen et al. 2014; Singh et al. 2014, 2011; Klein et al. 2011). TiO<sub>2</sub>-plain, TiO<sub>2</sub>-PVP, TiO<sub>2</sub>-F127, TiO<sub>2</sub>-AA4040, and CeO<sub>2</sub>-plain MNMs were from Promethean (Nottingham, UK) and were synthesised using a continuous-flow hydrothermal method which has been previously described in the literature (Lester et al. 2006, 2013). SiO<sub>2</sub>-un, SiO<sub>2</sub>-NH<sub>2</sub> and SiO<sub>2</sub>-COOH NPs were synthesised and characterised at JRC (Ojea-Jimenez et al. 2016). PS-NH<sub>2</sub> MNMs (Bangs Laboratory, Fishers, IN, USA) were used as positive control.

All participants in the present work received aliquots from the same batches of MNMs either in suspension or as dry powder, and used them as provided. A standard operating procedure (SOP) for dispersion of the MNMs and for exposure of cells was developed to maximise harmonisation across laboratories and hence minimise variations of the MNM suspensions. Briefly, MNMs were dispersed at 5 mg/mL in water, and then diluted to the dosing concentrations as described below except for hydrophobic MNMs, i.e. ZnO NM-111. For direct comparability, both ZnO NM-110 and ZnO NM-111 were dispersed according to the NanoGeno-Tox dispersion protocol (Jensen et al. 2011): To prepare a 2.56 mg/mL stock solution, 15.36 mg MNMs was weighed and then dispersed in 30 µL ethanol (> 96%). After gentle mixing 970 µL of 0.05% bovine serum albumin (BSA) in sterile filtered MilliQ water was added and the suspension was carefully mixed. Then, another 5 mL of 0.05% BSA solution was added (total volume 6 mL).

Suspensions which were prepared from MNM powder were ultrasonicated for 15 min in an ultrasonic bath (min 250 W), while those prepared from MNM suspensions were ultrasonicated for 5 min. JRC used a VialTweeter with 1.1 W/mL for ultrasonication. The stock suspensions were further diluted in the respective cell culture media, which contained 10% foetal bovine serum (FBS) which was centrally purchased as one lot (Gibco, Life Technologies, Darmstadt, Germany, Cat. number 10270–106, LOT-Number 41G1931 K). The FBS was distributed among all partners and was also used for the exposure of the different cell lines to MNMs to ensure biological reproducibility. All MNMs have been characterised under the respective experimental conditions in complete cell culture medium (DMEM or William's MediumE) immediately following dispersion (Time 0 h) and after 24 h at 37 °C (Time 24 h) (Tables 1, 2).

Dynamic light scattering (DLS) measurements were performed on a Malvern Zetasizer (nano ZS) at the University of Birmingham (UoB). Ten consecutive measurements were carried out and averaged to calculate the mean size. The results were obtained at 37 °C with samples equilibrated for 2 min before the measurements were started. Transmission Electron Microscopy (TEM) samples were prepared on copper grids by means of the drop method. MNM imaging was carried out using a JEOL 1200 TEM at an accelerating voltage of 80 kV.

### Cells and exposure to MNMs

HepaRG, a human hepatic stem cell line, was established and patented by INSERM (National Institute of Health and Medical Research) laboratory at Rennes, France. Undifferentiated HepaRG cells were provided by Biopredic International (Rennes, France) in cryopreserved vials. During cell maintenance, the cells were cultured in maintenance medium consisting of William's MediumE (Thermo Fisher Scientific, Melegnano, Italy) with 10% FBS (HyClone Fetal-Cone III, HyClone), 1% L-glutamine, 1% penicillin/streptomycin, 5 µg/mL bovine insulin and 50 µM hydrocortisone (all from Sigma, Milan, Italy). The cells were seeded at a density of  $1 \times 10^6$  cells into 75 cm<sup>2</sup> flasks and the medium was refreshed every 2 to 3 days. Upon confluence, the cells were transferred into 150 cm<sup>2</sup> flasks. After 14 days, the cells start to differentiate into hepatocytes and biliary cells. This process is supported by changing to differentiation medium, which consists of maintenance medium plus 1.7% DMSO (starting with 0.85% DMSO for 1 day). After 2 weeks in differentiation medium, the hepatocytes were selectively trypsinised and detached whereas the biliary cells remained adhered to the plate. The hepatocytes were then transferred into clear bottom black polystyrene 96-well microplates ( $5 \times 10^4$  cells/well in 100 µL) by an automated procedure.

HepG2 human hepatocellular carcinoma cells and RAW264.7 murine macrophages (both from ATCC, Rockville, MD, USA) were cultured in Dulbecco's Modified Eagle's Medium (DMEM) supplemented with 10% FBS, 100 U/mL penicillin and 100 mg/mL streptomycin (Life Technologies, Paisley, UK). For HT/C screening,  $5 \times 10^3$  cells were seeded in a clear flat bottom 96-well plate (Cell Star, Dublin, Ireland) in 100 µL of cell culture medium containing 10% FBS.

A549 human alveolar epithelial cells (ATCC, Rockville, MD, USA) were used by two partners but cultured differently. One partner (Ludwig Maximilians University, LMU) cultured the cells in modified Eagle's medium with Earle's salts (c-c-pro, Oberdorla, Germany) with 2 mM L-glutamine, and 10% FBS. Some hours before treatment, the cells were seeded at a concentration of  $8 \times 10^3$  cells per well on micro-patterned single cell arrays in 8 wells

(ibidi GmbH, Martinsried, Germany). The other partner (Karlsruhe Institute of Technology, KIT) cultivated the A549 cells in DMEM supplemented with 100 U/mL penicillin, 100 mg/mL streptomycin, 2 mM L-glutamine, and 10% FBS. HCT116 human colon epithelial wild-type (wt) and p53 knock-out cells (kindly provided by B. Vogelstein, John Hopkins University, Baltimore, USA) were cultivated in DMEM supplemented with 100 U/mL penicillin, 100 mg/mL streptomycin, and 10% FBS. One day before treatment, A549 and HCT116 cells were seeded into 96-well plates at a density of  $8 \times 10^3$  cells/well.

The medium for MNM exposure was DMEM for A549, HepG2, RAW264.7 cells and William's MediumE for HepaRG cells, both supplemented with 10% centralised FBS. Cells were exposed to MNM concentrations of 1, 2, 3.9, 7.8, 15.6, 31.2, 62.5, and 125 µg/mL which corresponds to cell surface area doses of 0.3, 0.6, 1.2, 2.4, 4.9, 9.8, 19.5, 39.1 µg/cm<sup>2</sup> for 24 h assuming that the total particle mass deposited on the cells. Due to their set-up using the HTS robot, one participant (JRC) used a quantitative high-throughput screening (qHTS) format which allowed inclusion of two additional concentrations (one higher and one lower than the above range, i.e. 0.5 and 250 µg/mL, respectively) with minimal extra effort. Pure medium was used as negative control and PS-NH<sub>2</sub> MNMs as positive control.

### HT/C assays

The screening workflow is slightly different in each of the participating laboratories; however, the principal steps are similar: cells are exposed to MNMs in multi-well microplates, usually 96-well plates. The different cell lines were stained after the defined exposure time with fluorescent dyes, which are specific for the biological endpoints to be tested. Subsequently, cells were imaged by an automated microscope, which allows acquisition of bright field images and the detection of different fluorescent signals at the same time. The imaging data are processed using specific image analysis software to generate quantitative data on viability status and other endpoints. Usually, heatmaps provide visually structured representations of the acquired data, which facilitates the comprehension and interpretation of large data sets. In the following, the specific assays and technology used in the different partner laboratories are briefly outlined.

#### *HT/C assays at JRC*

Hamilton Star and Starlet liquid handling platforms (Hamilton Italia Srl, Agrate Brianza, Italy) under a laminar hood with a 96-tip head were used to guarantee fully automated procedures throughout the experiment, from cell seeding to serial dilution preparation, plate treatment and staining.

Cell count, nuclear intensity and size, mitochondrial membrane potential and cell membrane damage are detected in parallel by automated staining and fixation using Hoechst 33342, the MitoHealth stain and Image-iT DEAD Green (Invitrogen, San Giuliano Milanese, Italy) and subsequent analysis using the Cellomics ArrayScan VTI HCS Reader (20× magnification) (ThermoFisher, Monza, Italy). The ArrayScan VTI has a robotic arm to load/unload the plates and can process tens of plates per experiment. For each experiment, about 30,000 images were taken and analysed using Thermo Scientific Cellomics iDEV High Content intelligent acquisition software. Cell number, nuclear shape and staining intensity by Hoechst 33342 (blue) serve as markers for cytotoxicity, red staining (MitoHealth stain) indicates mitochondria with intact membrane potential and green staining (Image-iT DEAD Green) indicates nuclei with damaged cell membrane.

Cleaved caspase-3 is detected by automated staining and fixation using an anti-active caspase-3 primary antibody (Anti-ACTIVE<sup>®</sup> caspase-3 pAb, rabbit polyclonal, Promega, Milan, Italy), followed by incubation with the fluorescent secondary antibody (Alexa fluo 488 goat anti rabbit, green). Detection of lipid accumulation was done by automated staining and fixation using the LipidTOX Green stain (HCS LipidTOX<sup>™</sup> Neutral Lipid Stains, Invitrogen, San Giuliano Milanese, Italy). Fluorescence was detected using the Cellomics ArrayScan VTI HCS Reader. Image analyses were performed by the Cellomics iDEV High Content intelligent acquisition software.

#### *HT/C assays at UCD*

After incubation with MNMs, Hoechst 33342 (400 nM) was used to identify the cell number and changes in nuclei area, tetramethylrhodamine methyl ester (TMRM, 20 nM) was employed to assess loss of MMP, LysoTracker green (50 nM) was used to assess reduction in pH inside the lysosomes (indicating an increase in the activity of the lysosome; the reduced pH activates proteases that attempt to digest the content of the lysosome) and TO-PRO<sup>®</sup>-3 (800 nM) was used to evaluate cell death as a result of plasma membrane permeabilisation. The cells were analysed using the ArrayScan VTI 740 at 20× magnification (Thermo Scientific, Dublin, Ireland). Data acquisition was configured to image an average of 300 to 500 cells within 10 acquired images. Analysis parameters were set according to the manufacturer's instructions and fixed thresholds were used for each parameter to separate background noise from fluorescence.

#### *HT/C assays at LMU*

LMU developed a new approach to assess cytotoxicity of MNMs. This single cell platform allows events in hundreds

of cells to be followed in parallel. Single cell arrays are obtained via micro-patterned structured surfaces, upon which cells self-organise into an ordered array (Röttgermann et al. 2014a, 2014b). In short, polydimethylsiloxane (PDMS) stamps were placed in 8well slides (ibidi GmbH, Martinsried, Germany) as a mask and selectively treated with oxygen plasma, 40 W for 3 min (Femto Diener, Ebhausen, Germany). The plasma exposed areas were passivated with 2 mg/mL PLL(20 k)-g(3.5)-PEG(2 k) (SuSoS AG, Dübendorf, Switzerland) in aqueous buffer (10 mM HEPES pH 7.4 and 150 mM NaCl). After removing the stamp the remaining parts were made cell adherent by exposure to 35 µg/mL fibronectin (YoProteins, Huddinge, Sweden) for 45 min.  $8 \times 10^3$  cells per well were seeded to achieve a filling of roughly one cell per adhesion site. The geometry of the square adhesion sites was  $30 \times 30 \mu\text{m}$  and the lattice distance was 90 µm. After an incubation of around 6 h to let the cells adhere the MNM solutions were mixed with the fluorescent markers in DMEM supplemented with 10% centralised FBS. Viability was detected via diluted (3%) caspase 3/7 marker (CellEvent Green, Life Technologies, Darmstadt, Germany) together with a nuclear stain (25 nM Hoechst 33342, Life Technologies, Darmstadt, Germany). Cell death was determined via the fluorescence signal of the PI staining solution (Novus Biologicals, Abingdon, UK). As a negative control culture media only was added while PS-NH<sub>2</sub> MNMs (100 µg/mL) were added as a positive control.

Images were recorded after 24-h incubation with MNMs using an inverted Nikon TI Eclipse microscope (10× magnifications, Düsseldorf, Germany). For each position, a phase contrast and three fluorescence images were taken. Filter sets were automatically switched (DAPI, GFP, PI). The microscope was equipped with a SOLA fluorescence lamp (Lumencor, Tuebingen, Germany) and a CCD camera (Clara, Andor, Belfast, UK). The cell culture slide was held at a constant temperature of 37 °C in an ibidi heating system (ibidi GmbH, Martinsried, Germany).

A background correction was applied to the raw images and identification of the regions of interest (ROI) was performed by lattice geometries in the bright field images per image position. The fluorescence of the single cell sites was analyzed with in-house-written ImageJ plugins and MATLAB. A semi-automated control was operated to avoid empty, displaced and multi-cell occupied wells, ensuring eligible single cell readout.

#### *HT/C assays at KIT*

Directly after exposure to MNM suspensions in 100 µL culture medium, cells were incubated with 0.3 µg/mL Hoechst 33342 and 0.5 µg/mL PI for 30 min at 37 °C and 5% CO<sub>2</sub>. Subsequently, four images per well were acquired using the automated fluorescence microscope IX81 (Olympus,

Hamburg, Germany) with a tenfold objective. Automated image analysis was carried out using the Olympus scan<sup>^</sup>R analysis software. The total number of cells was determined by counting the Hoechst-stained nuclei. The individual Hoechst signal intensities in combination with the PI staining were used to discriminate between the different stages of cell death. Whilst Hoechst 33342 can penetrate both viable and dead cells, PI can only enter those cells with a damaged cell membrane. Therefore, normal viable cells were defined as “Hoechst-positive” and “PI-negative”. Cells undergoing apoptosis are characterised by condensation of the chromatin resulting in intensive Hoechst staining and were thus called “Hoechst-intensive”. Necrotic cells were detected via the PI fluorescence signal, and show a normal nuclear staining but are PI positive. They are characterised by a swelling of the cell followed by permeabilization of the cell membrane. During the late stage of apoptosis, the DNA gets fragmented and permeabilization of the cell membrane takes place thus enabling the PI dye to enter the cells. Therefore, discrimination between early apoptotic cells (“Hoechst intensive” and “PI negative”) and late apoptotic cells (“Hoechst intensive” and “PI positive”) could be made (Donauer et al. 2012; Schreck et al. 2012; Marquardt et al. 2017). After classification of detected cells into the different stages of cell death, the different cell populations were calculated and displayed as total numbers of viable and dead cells as well as the percentage distribution of dead cells into the different stages of cell death.

For mechanistic follow-up studies, inhibitors of apoptosis (Q-VD-OPh, MP Biomedicals, Heidelberg, Germany), autophagy (3-methyladenine, 3-MA, Sigma-Aldrich, Taufkirchen, Germany) and soluble ZnCl<sub>2</sub> (Merck, Darmstadt, Germany), were used.

## Data analysis

The data analysis is based on the Signal to Noise Ratio (SNR, defined as the measured value minus the mean of the background and then divided by the background standard deviation) (Liu et al. 2013; Ling 2008). The obtained ratio can be easily compared across endpoints and labs. Another feature of the SNR is that it indirectly provides the significance of the signal and therefore no additional information is necessary for significance.

The following normalisation was applied to all datasets using SNR as the output:

1. For each MNM and each concentration, the average of the technical replica ( $X_c = (X_{c1} + X_{c2} + \dots + X_{ci})/i$ ) is calculated, where  $X_{ci}$  is the observation  $X$  at concentration/plate  $c$  and  $i$  stands for the  $i$ -th observation on the plate.

2. The average of the negative controls (medium only) per plate ( $\overline{NC_c}$ ) is calculated (given the qHTS format for JRC this leads to 10 different NC averages (one per plate)).
3. The noise of the plate is calculated by subtracting the plate average of the negative controls from the individual values ( $Noise_{ci} = NC_{ci} - \overline{NC_c}$ ).
4. The standard deviation of the noise ( $SD_c$ ) is calculated differently among the partners. JRC averages 10 different average negative controls (one for each plate) thus capturing the plate noise and 1 single general standard deviation capturing the variability of the noise (obtained from 40 observations, 4 per plate). KIT and UCD calculate  $SD_c$  from the negative controls per plate.

The SNR for each MNM at each concentration is finally calculated as:

$$SNR = \frac{X_c - \overline{NC_c}}{SD_c}$$

The aim was to identify MNMs exhibiting significant effects (up and/or down regulation) using the above normalised data for the different MNM concentrations and for different endpoints without using a parameterized model such as the Hill function to obtain an EC<sub>50</sub>. So, the null-hypothesis would be no effect from exposure to MNMs relative to the unexposed (medium only) control cells. Conclusions can easily be drawn comparing data to the threshold of  $-3$  (for downwards effect) and  $+3$  (for upwards effect). The value 3 is obtained from the hypothesis that the means of two normal distributed variables, with different numbers of observations and unknown, but equal, variance can be assumed to be equal. It, thus, takes into account the variance of the control and the MNMs. In cases where this condition is met it can be concluded (at a 95% level of confidence) that the MNM is inducing an effect (under the conditions defined by the experimental setup and the specific assay) (Liu et al. 2013). To strengthen the conclusion a second condition has also to be met, which is that significant effects will exceed this threshold for at least 2 consecutive concentrations. This simple test avoids that a single outlier is picked up as the first concentration showing a significant effect.

In the case of reconfirmation and follow-up experiments, results on cell death normalised to the total cell number are depicted as bar charts and are expressed as means + standard error of the mean (s.e.m.). The significance of the difference between two mean values was assessed by a two-tailed Student's  $t$  test. A  $p$  value  $< 0.05$  was considered to be statistically significant.

## Results

### Physical–chemical characterization of MNMs

The MNMs tested belong to the priority list of OECD reference materials (silver, titanium dioxide, cerium oxide, zinc oxide, silicon dioxide) as these MNMs are already in commerce with a high production volume. The selected library of different MNMs spans a size range of 5–90 nm and covers different core chemistries, coatings and surface functionalization (Table S1). The selected particles include SiO<sub>2</sub> (similar size of < 20 nm, different surface modifications), TiO<sub>2</sub> (similar size, different crystal structure and surface coatings), CeO<sub>2</sub> (different synthesis routes and thus different characteristics), Ag (surface coated), ZnO (similar size, hydrophobic coating or hydrophilic). PS-NH<sub>2</sub> MNMs were included as positive control. The TEM-derived diameters confirm that all particles are in the nanometer range. Z-average and polydispersity index (PDI) were determined in William's MediumE (Table S1) as well as in DMEM cell culture medium (Table S2) directly after preparing the suspension and after 24-h incubation under cell culture conditions. The agglomeration of the MNMs differs depending on the medium and time. Interestingly, apart from silver and plain silica MNMs, all other MNMs agglomerated in William's MediumE. However, MNM stability clearly differed in DMEM. For instance, PS-NH<sub>2</sub>, all TiO<sub>2</sub> MNMs except for NM-104 and ZnO (NM-110, NM-111) showed less agglomeration in DMEM, whereas CeO<sub>2</sub> (NM-212) and TiO<sub>2</sub> (NM-104) from the JRC repository were again present as larger agglomerates, similar to the sizes when suspended in William's MediumE. These findings highlight the necessity to characterise MNM suspensions in all relevant exposure media, which profoundly affect their stability and thus exposure dose.

Further physical–chemical characterization data of the MNMs under study can be found in NanoMILE Deliverable report D2.5, which is available upon request and from which a summary paper is currently in preparation. Detailed reports are also available on the physical–chemical properties of the representative MNMs TiO<sub>2</sub> (NM-103, NM-104) (Rasmussen et al. 2014), CeO<sub>2</sub> NM-212 (Singh et al. 2014), ZnO (NM-110, NM-111) (Singh et al. 2011), and Ag NM-300 K (Klein et al. 2011) from the JRC repository.

### MNM toxicity is dependent on dose, cell type and chemical composition

The selected MNMs were tested *in vitro* to link the physical–chemical properties to multiple adverse effects in a panel of cell lines derived from different organs (Fig. S1). The assays used to assess toxicity are based on HT/C imaging techniques. Endpoints such as viable cell count, cell

membrane permeability, markers of apoptotic cell death, mitochondrial membrane potential and lysosomal acidification were studied as indicators of acute cytotoxicity. In addition, cell type-specific adverse outcomes (i.e. hepatocyte-specific steatosis), which might be involved in MNM toxicity to a selected organ, were also included (Table S5). Soluble metal/metal oxide MNMs, specifically Ag and both ZnO MNMs, were most effective in reducing the number of viable cells in all different cell models, and had similar efficacy to the PS-NH<sub>2</sub> MNMs which were used as positive control (Fig. 1). Hydrophobic coating of ZnO MNMs diminished the noxious impact in some (HepG2 hepatocytes and macrophages), but not all, cells. However, ceria and silica MNMs were nearly ineffective in most cell lines over the dose range assessed. Interestingly, some MNMs triggered cell type-specific toxicity. TiO<sub>2</sub> MNMs in the crystal form of anatase, but not rutile, were toxic primarily to differentiated HepaRG liver cells, whereas other cell lines including undifferentiated hepatocytes (HepG2) were less affected. In the case of plain SiO<sub>2</sub> MNMs, RAW264.7 macrophages were selectively vulnerable. Functionalization of the silica surface by either amine- or carboxyl-modification suppressed the toxicity, presumably by reducing the number of surface-active silanol groups. In essence, MNM toxicity is influenced by chemical composition, surface coating and functionalization and also depends on the cell line investigated. When comparing the response of various cell lines

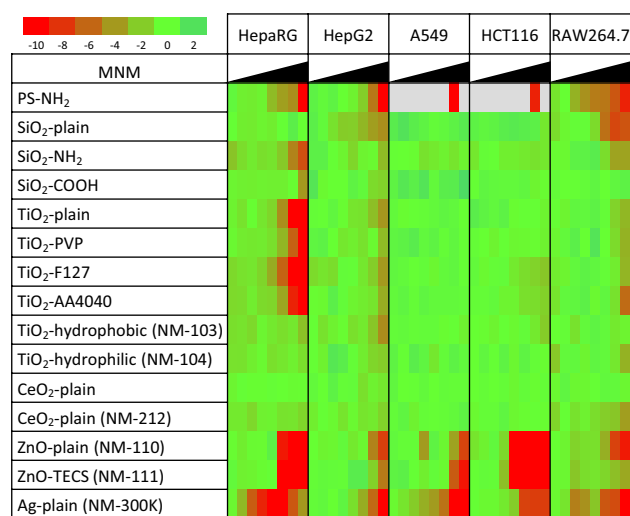


**Fig. 1** MNMs reduce viable cell counts dependent on dose, cell type and chemical composition. Cells were exposed to MNM concentrations between 1 and 125 µg/mL for 24 h, then stained with Hoechst 33342 for total cell number and a cell impermeable dye to identify cell membrane damage. Dead cells were subtracted from total cell count which was normalised to the untreated control. The data are presented in a heatmap depicting SNR. Colour code ranges from green to red indicating either a slight increase (dark green) or strong decrease of viable cells (red)

after exposure to different concentrations of multiple MNMs usually the nominal, i.e. applied mass concentration is used as a metric to establish dose response curves. However, the actual delivered dose can be accurately calculated by computational models considering the effective density and size of MNMs (DeLoid et al. 2014, 2015, 2017). Indeed, the Relative In Vitro Dose (RID) delivered to the cells varies significantly for the different MNMs (Tab. S3). After normalisation, the pronounced toxicity of PS-NH<sub>2</sub> is reduced compared to, e.g. SiO<sub>2</sub> or TiO<sub>2</sub> MNMs (Fig. S2). Also, the enhanced sensitivity of HepaRG cells towards TiO<sub>2</sub> MNMs is clearly diminished. Obviously, when performing HT/C assays appropriate consideration of the RID supports hazard ranking of MNMs across multiple endpoints and cell lines. As cells are usually exposed as monolayers, MNM effects on single cells were also addressed. Interestingly, A549 cells are much more sensitive towards MNM exposure when grown in isolation, demonstrating an important impact of cell density and cell–cell contacts when assessing MNM toxicity (Fig. S3). To gain further insights into cell type-specific mechanisms and actions of MNMs, multiple endpoints, as outlined above, were investigated which are described in the following sections.

### Impact of MNMs on multi-parametric read-outs in differentiated HepaRG liver cells

Upon systemic MNM exposure, the liver is one of the main target organs for their accumulation and thus a site susceptible to induction of adverse effects. The differentiated human hepatoma cell line HepaRG was, therefore, used

as a cell culture model to study a wide range of adverse effects of the different MNMs (Fig. 2): loss of mitochondrial membrane potential, caspase-3 activation, nuclear size and intensity (all indicative of apoptotic cell death), lipid droplet formation (indicative of steatosis which is an infiltration of liver cells with fat, associated with a disturbance of the metabolism), cell membrane damage and reduction of cell counts. As already shown in Fig. 1 for viable cell count, Ag MNMs were the most toxic MNM tested, as they affected all endpoints at very low concentrations (1.95–15.6 µg/mL). Interestingly, the Ag MNMs induced peak effects around concentrations of 15.6 and 32.3 µg/mL for most read-outs (Fig. S4). At higher concentrations, however, all readings return close to control levels. One possible explanation might be a dose-dependent difference in MNM aggregation/agglomeration or solubility, which could influence the deposited cellular dose and warrants further investigation. Analysis of the dose response (Fig. 2) and the lowest adverse effect levels (LOAELs) (Fig. S5) of all markers indicates a critical role of caspase-3 activation in cell death provoked by Ag MNMs.

Similar to Ag MNM, low concentrations of ZnO MNMs also affected various markers of cell death including caspase-3 activation. Hydrophobic surface coating by triethoxycaprylsilane did not suppress ZnO MNMs toxicity. In contrast to all other MNMs tested, both zinc oxide MNMs increased lipid droplet size, which goes along with earlier findings on pigs that were fed with a high concentration of zinc oxide in the diet. Hepatocytes of those pigs showed an increase in lipid accumulation, together with high hepatic

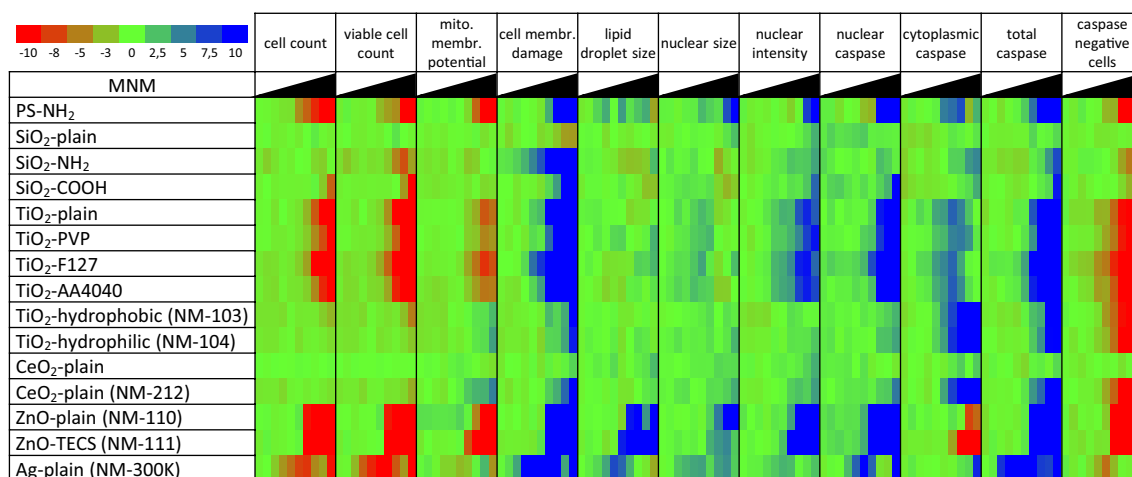


**Fig. 2** MNM effects in differentiated HepaRG liver cells on markers of cell death and steatosis. Cells were exposed to MNM concentrations between 0.5 and 250 µg/mL for 24 h, stained with endpoint-specific dyes [Hoechst (cell number, nuclear intensity and size), MitoHealth (mitochondrial membrane potential and cell membrane damage), Image-iT DEAD Green (nuclei with damaged nuclear

membrane), Caspase-3 (total, cytoplasmic, nuclear localisation and negative), LipidTOX Green (lipid droplet size/lipid accumulation)] and analyzed using the Cellomics ArrayScan VTI HCS Reader. Data are presented in a heatmap depicting SNR. Colour code ranges from green to red indicating a shift from no effect to a decrease of effect (red). A shift to blue indicates an increase of the effect



Zn concentrations (Jensen-Waern et al. 1998). Therefore, the effect found in our study might be a consequence of the high solubility of ZnO MNMs.

TiO<sub>2</sub> MNMs with the crystal form of anatase, but not rutile, initiated cell death accompanied by signs of membrane damage and caspase-3 activation; however, the various polymeric surface coatings had no impact on the strength of the response of the various Promethean TiO<sub>2</sub> MNMs. The MNMs produced by JRC (TiO<sub>2</sub> NM-103 and NM-104) equally induced an increase in caspase-3 activation. However, this was rather mild, as activated caspase-3 was mainly located in the cytoplasm, a marker of early apoptosis as discussed above. This further supports the overall slightly less adverse effects of these MNMs to HepaRG cells, compared to the Promethean TiO<sub>2</sub> MNMs. Ceria and silica MNMs showed largely no effect on the HepaRG cells. PS-NH<sub>2</sub> MNMs also affected caspase activation, mitochondrial membrane permeability and cell membrane integrity. Again, when data are normalised to the calculated deposited dose, the relatively high toxicity of PS-NH<sub>2</sub> MNM is greatly reduced (Fig. S6). Thus, the more detailed follow-up studies employing multiple markers of cell death suggest apoptotic events as key for the observed cytotoxicity of soluble (Ag and ZnO MNMs) and TiO<sub>2</sub> MNMs in HepaRG cells.

### Impact of MNMs on multi-parametric read-outs in HepG2 liver cells and RAW264.7 macrophages

The positive control (PS-NH<sub>2</sub> MNMs) enhanced nuclear condensation, mitochondrial depolarisation, lysosomal

acidification and plasma membrane permeabilisation suggesting HepG2 cells undergo apoptosis (Figs. 3, S7). This is in accordance with previous results, in which these MNMs were demonstrated to induce caspase-9-mediated apoptosis as a result of lysosomal rupture, leading to mitochondrial permeabilisation via Bcl-2 proteins and nuclear condensation, followed by plasma membrane permeabilisation, confirming apoptosis (Anguissola et al. 2014).

The TiO<sub>2</sub> MNMs showed no alteration in most parameters tested, up to 125 µg/mL, with no significant effect on nuclear morphology, mitochondrial membrane potential, or plasma membrane permeability. However, an increase in lysosomal acidification was observed in a dose-dependent manner for all TiO<sub>2</sub> MNMs in HepG2 cells, irrespective of their surface coating or crystal structure. Compared to the level of lysosomal damage inflicted by the PS-NH<sub>2</sub> positive control MNMs, TiO<sub>2</sub> MNM exposure might not exceed a critical threshold of lysosomal injury to subsequently trigger cell death. It should also be taken into consideration that HepG2 cells, due to their function as hepatocytes, have high trafficking capabilities and therefore, the increase in lysosomal stained compartment activity may be due to intracellular processing of MNMs at high doses, which may explain the plateau formed (as compared to the sharp decrease due to lysosomal rupture which is observed after acidification in the case of the PS-NH<sub>2</sub> MNMs).

Whereas CeO<sub>2</sub> and SiO<sub>2</sub> MNMs were almost without effect, the soluble Ag and ZnO MNMs were most potent in inducing cytotoxicity with features of apoptosis such as

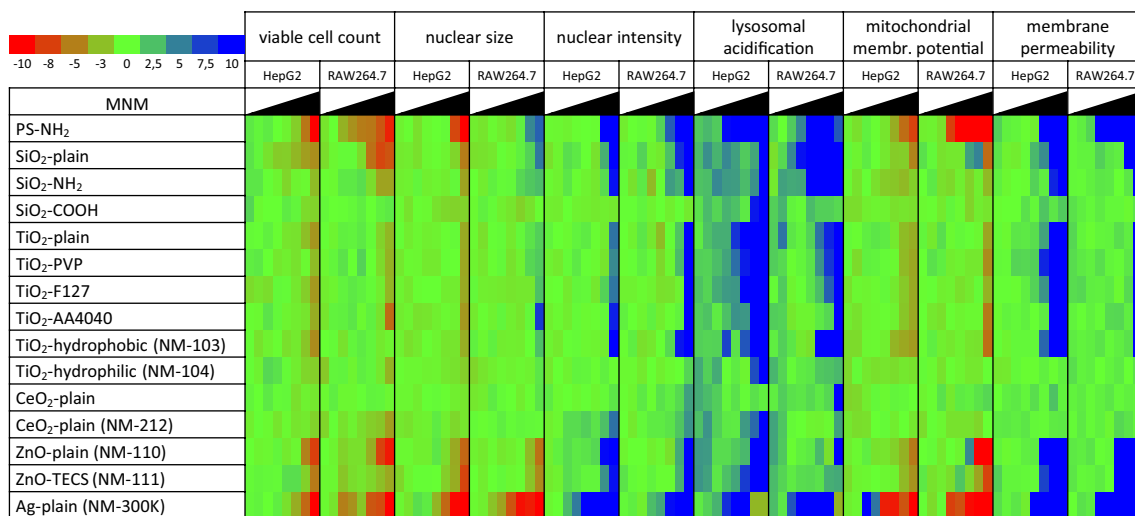


**Fig. 3** MNM effects in HepG2 liver cells and RAW264.7 macrophages on markers of cell death and lysosomal acidification. Cells were exposed as described in Fig. 1, stained with endpoint-specific dyes [Hoechst 33342 (cell count, nuclei size, nuclear intensity), TMRM (loss of mitochondrial membrane potential), LysoTracker green (Lysosomal acidification) and TOPRO3 (plasma membrane

permeabilisation)] and analyzed using the Celloomics Arrayscan VTI 740. Data are presented in a heatmap depicting SNR. Colour code ranges from green to red indicating a shift from no effect to a decrease of effect (red). A shift to blue indicates an increase of the effect

shrinkage of nuclei, enhanced DNA condensation and loss of mitochondrial membrane polarisation (Figs. 3, S7).

In RAW264.7 macrophages, the positive control PS-NH<sub>2</sub> MNMs induced nuclear swelling, as opposed to condensation, indicating that the cells were undergoing necrosis as demonstrated in (Anguissola et al. 2014), accompanied by mitochondrial depolarisation, increased area in the lysotracker stained compartment and increased plasma membrane permeabilisation. Plain SiO<sub>2</sub> MNM triggered a similar cascade of events whereby surface functionalization by either amine-modification or even more pronounced by carboxylation decreased toxicity. Although amine-modified silica MNMs appeared to be slightly less stable compared to plain silica MNMs (Tabs. S1, S2), carboxylated silica MNMs show a similar size, suggesting a dominant role of surface properties for toxicity. Lysosomal acidification was not observed to the same extent after exposure of macrophages to TiO<sub>2</sub> MNMs, when compared to HepG2 cells. None of the TiO<sub>2</sub> MNMs even at the highest concentrations showed strong toxicity as assessed by the number of viable cells in RAW264.7 cells. Similarly, CeO<sub>2</sub> MNMs did not provoke clear adverse responses. As observed in HepG2 cells, RAW264.7 cells were highly sensitive to Ag and ZnO MNMs, which again initiated cell death reminiscent of apoptosis.

Overall, together with the positive control PS-NH<sub>2</sub>, soluble Ag and ZnO MNMs were again the most toxic in both cell lines. However, after normalisation to the deposited dose, the relative modest toxicity of some TiO<sub>2</sub> MNMs becomes more pronounced whereas the more potent effects of PS-NH<sub>2</sub>, ZnO and Ag MNMs are alleviated (Fig. S7). Of note, SiO<sub>2</sub> MNMs specifically affected viability of macrophages dependent on surface properties by a mode of action similar to PS-NH<sub>2</sub> MNMs.

### **TiO<sub>2</sub> and soluble Ag and ZnO MNMs evoke cell death in A549 lung and HCT116 colon cells**

As soluble Ag and ZnO MNMs reduced viable cell counts in A549 lung cells and HCT116 colon cells, whereas some TiO<sub>2</sub> MNMs selectively affected HCT116 cells (Figs. 1 and S2) more detailed follow-up studies on the mode of cytotoxicity were performed. As expected, none of the TiO<sub>2</sub> MNMs triggered prominent cell death in A549 cells, yet in HCT116 cells some TiO<sub>2</sub> MNMs (i.e. those with anatase crystal structure) showed moderate cytotoxicity (Fig. 4a) which is even more evident when data are normalised to the deposited dose (Fig. S8).

Clearly, as observed for other cell lines above, soluble Ag and ZnO MNMs were most potent to induce cell death in A549 and HCT116 cells with the latter being more sensitive (Fig. 4a). The LOAEL for Ag MNMs to provoke cell death in A549 cells was 31.3 µg/mL compared to 7.8 µg/

mL to reduce cell number (Figs. 4b, S9c) indicating that at low doses inhibition of cell proliferation precedes cell death initiated at high concentrations. Furthermore, the pattern of cell death induced by Ag MNMs is characterised by late apoptotic and primarily necrotic cells. Moreover, Ag MNMs induced an atypical nuclear morphology at cytotoxic concentrations (Fig. S9b). Although some classical signs of apoptosis such as partial DNA condensation and disintegration of nuclei were evident, the area of DNA staining is heavily enlarged and not condensed as expected for apoptotic cells (Fig. S9b). As the integrity of the cell membrane was already compromised, witnessed by concomitant PI staining and no cellular fragmentation and blebbing being observed, damage by Ag MNMs presumably elicited initially apoptosis which was prematurely terminated to result in necrosis. This was even more pronounced in HCT116 cells, where Ag MNMs dose-dependently blocked proliferation and induced a mixed mode of accidental cell death at high MNM concentrations (Fig. S9c).

Both ZnO MNMs induced concentration-dependent cell death in both lung (A549) and colon (HCT116) cells which correlates with reduced total cell counts (Figs. 4c, S9d–f). Hence inhibition of proliferation at lower concentrations, as documented above for Ag MNMs, does not occur in the case of ZnO MNMs, suggesting that an adaptive response to allow for detoxification might be specific for certain soluble metal MNMs only. Colon cells were even more susceptible to ZnO MNMs as cytotoxic effects were more pronounced, observed at lower concentrations and accompanied by an increase in late apoptotic and necrotic cells (Fig. S9f). Hydrophobic surface modification of ZnO MNMs rendered A549 but not HCT116 cells more sensitive to MNM exposure (Figs. 4c, S9f). In contrast, the increased sensitivity of A549 cells towards hydrophobic ZnO MNM disappeared whereas HCT116 cells seem to be even more vulnerable towards hydrophilic ZnO MNMs after considering the deposited dose (Fig. S8). Toxicity is likely mediated by the release of Zn ions from the MNMs, as ZnCl<sub>2</sub> at equimolar Zn concentrations showed, although more pronounced, qualitatively similar cytotoxic effects (Fig. 4c).

### **Mechanistic investigation of TiO<sub>2</sub> MNM-induced cytotoxicity in HCT116 colon cells**

As anatase TiO<sub>2</sub> MNMs provoked cell death in HCT116 colon cells (Fig. 4), we further investigated the underlying molecular mechanisms, specifically a potential role of p53 in MNM-induced apoptosis. The transcription factor and tumour suppressor protein p53 is activated due to cellular stress and activates different cellular signalling cascades which regulate cell growth, cell cycle progression and apoptosis (Menendez et al. 2009; Efeyan and Serrano 2007). Exposure of HCT116 wt cells to TiO<sub>2</sub>-F127 MNMs

**Fig. 4** Metal and metal oxide MNMs induce cell death dependent on dose and cell type in A549 lung cells and HCT116 colon cells. Cells were exposed as described in Fig. 1, stained with Hoechst and PI and analyzed using an automated Olympus IX81 microscope and scan<sup>R</sup> Acquisition software. **a** Comparison of cell death rate in A549 and HCT116 cells after exposure to various metal and metal oxide MNMs. Note the enhanced sensitivity of HCT116 cells. Data are presented in a heatmap depicting percentage of cell death. Colour code ranges from green over blue to red indicating a shift from no effect to an increase of cell death. **b** Cell death caused by Ag MNMs in A549 cells primarily resembles necrosis with some minor proportion of apoptosis. **c** ZnO MNM-provoked cell death in A549 cells is dominated by apoptosis and is dependent on surface coating. ZnCl<sub>2</sub> solutions at equimolar concentrations of Zn were used for comparison. Data represent mean + s.e.m. of 3 (ZnO plain/TECS) and 2 (ZnCl<sub>2</sub>) independent experiments with 3 technical replicates each (\*\**p* < 0.001, \*\**p* < 0.01, \**p* < 0.05)

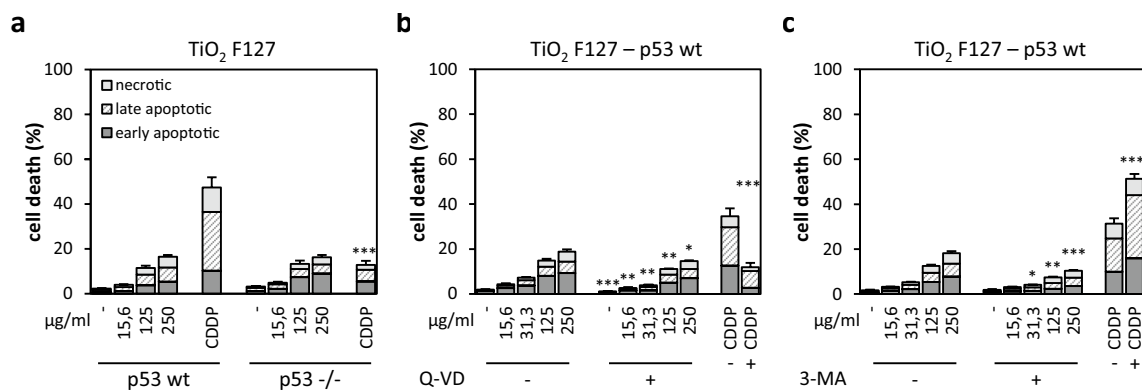
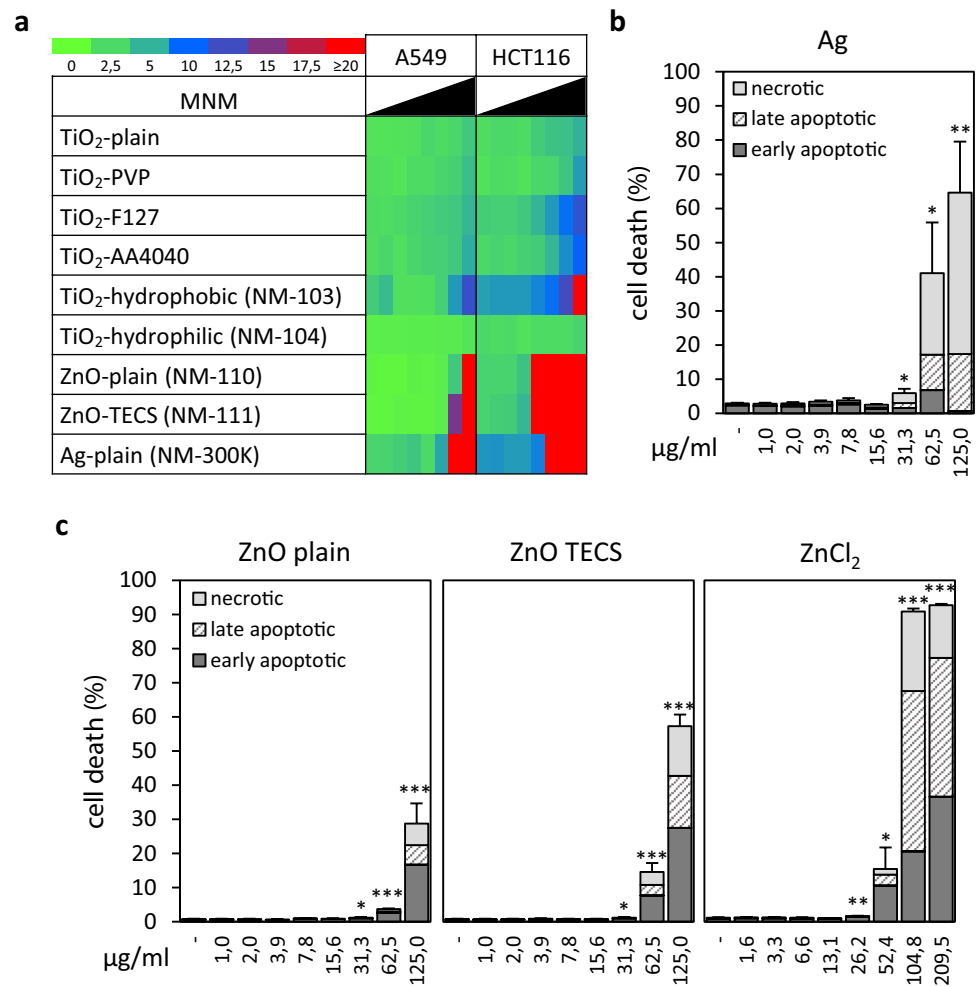


**Fig. 5** Mechanistic investigation of TiO<sub>2</sub>-F127 MNM-induced cytotoxicity in HCT116 colon cells. **a** In contrast to the positive control cisplatin (CDDP, 50 µM), TiO<sub>2</sub>-F127 MNM-induced apoptosis is independent of p53. HCT116 p53 wildtype (wt) and p53<sup>-/-</sup>-deficient cells were incubated with the indicated concentrations of MNMs for 24 h and the percentage of the different modes and stages of cell death are displayed. **b, c** Inhibition of caspases and autophagy par-

tially reduce apoptosis in response to TiO<sub>2</sub>-F127 MNMs. HCT116 wt cells were pretreated with **(b)** the pan-caspase inhibitor Q-VD (10 µM, 30 min) or **(c)** autophagy inhibitor 3-MA (4 mM, 30 min), followed by MNM exposure for 24 h. Analysis was performed as described in Fig. 4. Data represent mean + s.e.m. of 2 independent experiments with 3 technical replicates each (\*\**p* < 0.001, \*\**p* < 0.01, \**p* < 0.05)

induced apoptosis, which, however, was not diminished in p53 knock-out cells (Fig. 5a). Nevertheless, cell death progression was delayed in p53-deficient cells, as an increase in early apoptotic and a concomitant decrease in late apoptotic cells was observed. Similar results were obtained for plain TiO<sub>2</sub> MNMs (Fig. S10a). Lack of an essential role for p53 in TiO<sub>2</sub> MNM-induced cell death is also supported by the absence of p53 up-regulation at the protein level (Fig. S10b). The involvement of caspases was also investigated as they are essential for initiation and execution of apoptotic cell death. Inhibition of caspases slightly reduced the cytotoxicity due to TiO<sub>2</sub> MNM exposure (Figs. 5b, S10c). Finally, the role of autophagic processes in the observed cytotoxicity was studied. Autophagy is a conserved process, primarily cytoprotective, yet also known to contribute to cell death (Stern et al. 2012; Zhao et al. 2013; Marquardt et al. 2017). Indeed, the autophagy inhibitor 3-methyladenine (3-MA) decreased cell death in response to TiO<sub>2</sub> MNMs (Figs. 5c, S10d).

## Discussion

Here, a range of MNMs with different core chemistries and surface modifications was investigated to link their physical–chemical properties to multiple adverse effects in various cell lines from different organs. Microscopy-based high-throughput screening assays were applied to enable multi-parametric analysis of adverse effects from exposure to the MNMs. While no major surprises emerged in terms of the acute toxicity of the MNMs dependent on their chemistry, the study confirms a lot of previous data from smaller, fragmented datasets, thereby increasing confidence in the use of various HT/C assays to assess acute toxicity of MNMs.

The selective toxicity of metal bearing MNMs (silver, zinc oxide), which may at least in part, be linked to the release of metal ions, has been confirmed. Furthermore, TiO<sub>2</sub> MNMs with the anatase crystal structure triggered cell death in some but not all cell types. Moreover, SiO<sub>2</sub> MNMs specifically affected macrophages dependent on their surface functionalization. Also the use of PS-NH<sub>2</sub> MNMs as a positive control MNM emerged as a reasonable approach, as adverse effects of these MNMs could be detected in all cellular systems. The most striking finding from this study is the critical role of cell type in the response to MNMs.

Quite often, due to differences in exposure conditions, various methods to prepare MNM suspensions and diverse suppliers of MNMs, results on toxicity are often contradictory. Therefore, in this work the same MNMs, dispersed using a standardised protocol and serum from a single batch, and exposed to the cells in an identical manner, were assessed allowing the identification of cell type-specific

responses. Interestingly, the differentiated liver cell line HepaRG seems to be most sensitive to MNMs, whereas non-differentiated HepG2 hepatoma cells were more resistant. Possibly, differentiation of liver cells might determine the susceptibility to MNMs, an issue not well studied so far in the field of nanotoxicology. Interestingly, recent studies performed with differentially polarised macrophages also suggest a clear impact of differentiation on MNM uptake and response (Jones et al. 2013; Hoppstädter et al. 2015).

Four main pathways for MNM toxicity are currently recognised (Gebel et al. 2014; Lynch et al. 2014): (a) the release of toxic chemical constituents from MNMs (e.g. Cd from quantum dots or ionic silver from Ag MNMs)—i.e. MNM dissolution, (b) the direct effects from physical contact with MNMs, influenced by their size and shape, and surface properties and which produce interferences with important biological functions for example by altering conformation of biomolecules—i.e. MNM surface effects, (c) the inherent properties of the material, such as photochemical and redox properties resulting from bandgap or crystalline form—i.e. structure effects, and (d) the capacity of MNMs to act as vectors for the transport of other toxic chemicals to sensitive tissues—i.e. MNM Trojan horse effects. Once a MNM encounters a cell or an organism, toxicity could occur through one or a combination of these mechanisms.

Assigning the toxic MNMs of our library to the various categories, metal-based soluble Ag and ZnO MNMs would fit into the first group and were toxic in all cell lines, which is in accordance with published data (Deschamps et al. 2014; Dilger et al. 2016; Piret et al. 2017). Dispersion of Ag MNMs in biological media will lead to surface oxidation and release of Ag<sup>+</sup> (Reidy et al. 2013; Kim and Tanguay 2014). Ag MNMs inhibit cell proliferation by interacting with membrane proteins and disturbing signalling pathways. The MNMs can also induce mitochondrial dysfunction, driving generation of ROS and thereby damage to proteins, lipids and nucleic acids. Since silver, either as ion or as MNM, has a strong affinity to sulphur, an important mechanism of toxicity is the interaction of Ag with sulphur-containing macromolecules such as proteins (Johnston et al. 2010).

ZnO MNMs are also toxic in mammalian systems (de Vandebriel and Jong 2012), especially when they are inhaled. Accidental inhalation of ZnO MNMs can induce metal fume fever in human subjects, a syndrome which is common among welders (Gordon and Fine 1993). Like Ag MNMs, ZnO MNMs are partly soluble in medium and within cells. Zinc is an abundant and essential transition metal in biological systems and plays an important role, e.g. in the maintenance of protein structure and enzymatic function. However, free Zn<sup>2+</sup> ions are toxic and are, therefore, bound to Zn-binding proteins such as metalloproteins. Zn is known to be a redox-inert metal, which does not participate in oxidation–reduction reactions (Valko et al. 2006).

However, due to its interaction with cysteine thiols, it plays an important role in redox signalling and kinase- or phosphatase-related signal transduction (Wu et al. 2013). ZnO MNM uptake into endosomes and their final destination in acidifying lysosomes accelerates their dissolution. The intracellular Zn ions induce lysosomal and mitochondrial damage, resulting in induction of ROS and cytokine release (Cho et al. 2011). Lysosomal swelling in HepG2 and RAW264.7 cells could be identified as an early marker after exposure to Ag but not ZnO MNMs in our studies. Incubation of cells with PS-NH<sub>2</sub> MNMs also induced lysosomal swelling and rupture, demonstrating a key role of this organelle for MNM injury pathways.

Adverse effects have also been reported for insoluble TiO<sub>2</sub> MNMs mainly in the form of anatase, in accordance with our results. These MNMs would belong to the third category, i.e. structure effects dominating the cellular response (Sayes et al. 2006). There are indeed contradictions in the literature about the toxicity of TiO<sub>2</sub> MNMs, with both positive and negative results, presumably due to differences in coatings, crystal structure and sizes, as well as differences due to exposure conditions (e.g. different media). Some studies showing cytotoxicity and/or genotoxicity indicate that this occurs under certain circumstances, and that in *in vitro* experiments, this is dependent on cell type, crystal phase and concentration of TiO<sub>2</sub> MNMs (Johnston et al. 2009). For example, in our previous studies, we observed very low responses to TiO<sub>2</sub> MNMs, e.g. in A549 alveolar epithelial cells and RAW264.7 macrophages (Panas et al. 2013). Others have demonstrated a TiO<sub>2</sub> MNM-induced dose- and time-dependent decrease in cell viability, caspase-3 activation and DNA condensation indicative of apoptosis (Park et al. 2008; Shi et al. 2010) in BEAS-2B bronchial epithelial cells, similar to our current findings. ROS production and glutathione depletion, increased heme oxygenase-1 (oxidative mechanism), IL-8, IL-1, IL-6, TNF- $\alpha$ , and CXCL2 expression (inflammatory response) were also observed. Lysosomal membrane damage and lipid peroxidation might also contribute to TiO<sub>2</sub> MNM-induced cell death (Hussain et al. 2010). Non-toxic doses of TiO<sub>2</sub> MNMs induce DNA damage, in particular after long-term exposure (Armand et al. 2016). Also in animal models numerous adverse effects have been documented. Notably, and based on such evidence, both International Agency for Research on Cancer (IARC) and National Institute for Occupational safety and Health (NIOSH) have classified TiO<sub>2</sub> MNMs as a possible carcinogen for humans (Shi et al. 2013; Sha et al. 2015). The European Chemicals Agency (ECHA) has also published a report in 2016 which proposes to classify TiO<sub>2</sub> MNMs as “potentially carcinogenic to humans” (category 1B)/“may cause cancer by inhalation” (ECHA 2016).

Mechanistic studies performed in the present work on the mode of cytotoxicity demonstrated that anatase TiO<sub>2</sub> MNMs

initiated apoptotic cell death in HepG2 and HepaRG hepatocytes as well as in HCT116 colon cells. In the latter cell line a role of caspases and autophagy but not of p53 could be identified. TiO<sub>2</sub> MNMs are used, e.g. as food supplements (TiO<sub>2</sub> E171, 36% of particles by number are smaller than 100 nm and can be purchased as rutile or anatase) and in pharmaceutical products (Weir et al. 2012). As reported for animals, orally administered TiO<sub>2</sub> MNMs are absorbed in the gastro-intestinal tract and accumulate in the liver, spleen, kidney and lung and may cause tissue damage at high doses (Jovanovic 2015). Direct absorption of pharmaceutical/food grade TiO<sub>2</sub> particles from the gastrointestinal tract into the blood stream has also been demonstrated in healthy human volunteers (Pele et al. 2015). Therefore, further *in vivo* studies are warranted to address the fate and biological activity of TiO<sub>2</sub> MNMs specifically in the digestive tract and in the liver under realistic exposure conditions.

SiO<sub>2</sub> and PS-NH<sub>2</sub> MNMs belong to the second group of surface-active MNMs. PS-NH<sub>2</sub> MNMs are known to induce cytotoxicity at low concentrations leading to apoptosis. Therefore, PS-NH<sub>2</sub> MNMs have been used to study the toxic mechanism of action. In RAW264.7 macrophages, but not in BEAS-2B bronchial epithelial cells, PS-NH<sub>2</sub> MNMs initiated lysosomal injury explained by the so-called proton sponge hypothesis (Xia et al. 2008). After uptake into lysosomes, the amine groups bind protons with high affinity. This leads to exaggerated activity of the proton pump leading to chloride influx, osmotic swelling and rupture of the lysosome. Indeed, lysosomal permeabilisation and toxicity could be prevented by addition of bafilomycin A1, an inhibitor of v-ATPase which prevents endosomal acidification. These events were not observed in BEAS-2B cells; however, the PS-NH<sub>2</sub> MNMs also induced mitochondrial damage, ATP depletion and cytotoxicity (Xia et al. 2008).

The sequence of events leading to PS-NH<sub>2</sub> MNMs induced cell death has been elucidated in detail in astrocytoma cells (Wang et al. 2013a) as follows: increase of lysosomal volume—increased ROS levels—loss of lysosomal integrity—shrinkage of cell size—loss of mitochondrial membrane potential—loss of plasma membrane integrity—cell death. The impairment of mitochondria marks the point of no return for cell death. It has further been shown that the biomolecular corona of the PS-NH<sub>2</sub> MNMs is retained during the MNM uptake into the cell until they reach the lysosomes where the corona is degraded (Wang et al. 2013b). In a HT/C screening assay additional cell types (HEK293, HepG2, hCMC/D3, A549, SHSY5Y, 1321N1, RAW264.7) were tested for their EC<sub>50</sub> values for the different endpoints as a basis for determining the sequence of PS-NH<sub>2</sub> MNM-induced events (Anguissola et al. 2014). All cell lines besides RAW264.7 macrophages had the same sequence, with: lysosomal acidification, mitochondrial depolarisation, and simultaneous nuclear condensation, cytosolic calcium

increase and plasma membrane permeabilization. These endpoints are indicators of apoptosis, which is in line with our current findings. Instead of nuclear condensation, in RAW264.7 cells a dose-dependent nuclear swelling was observed, which is an indicator of necrosis.

For uncoated SiO<sub>2</sub> MNMs, a similar response pattern as documented for PS-NH<sub>2</sub> MNMs was evident in RAW264.7 macrophages, indicating a critical role of lysosomal injury for cytotoxicity. Surface modification (–COOH and –NH<sub>2</sub>) suppressed toxicity as reported previously also by others (Yamashita et al. 2011; Morishige et al. 2012) and might be related to the reduction of surface-active silanol groups. Apart from macrophages, all other epithelial cell lines were rather resistant to SiO<sub>2</sub> MNMs (plain or surface charge modified) which is likely due to the protective effect of the protein corona by passivation of the silica surface (Al-Rawi et al. 2011; Panas et al. 2013). Therefore, the cell type-specific toxicity of SiO<sub>2</sub> MNMs might be related to enhanced MNM uptake and subsequent disturbance of the endo-lysosomal compartment in macrophages.

Yet, some MNMs did not score in our assays, namely CeO<sub>2</sub> NM-212, although in the lung of rats the same material provokes inflammation and cytotoxicity after inhalation (Keller et al. 2014). The apparent difference in the outcome of the in vitro and in vivo experiments for CeO<sub>2</sub> MNMs might be resolved by adapting and improving the in vitro systems, e.g. by using co-cultures of epithelial cells and macrophages and by performing exposure at the air–liquid interface (ALI). An ALI exposure system is an advanced in vitro system to deposit MNMs from an aerosol directly onto cells, an approach which closer simulates the conditions in the lung (Mülhopt et al. 2009; Panas et al. 2014).

Future studies on mechanisms of MNM toxicity should focus on the identification of the MIEs such as the disturbance of lysosomal integrity, which might not only be essential for downstream acute cytotoxicity but presumably also drive other adverse outcomes in different settings. As more and more adverse outcome pathways are described, HT/C screening needs to capitalize on molecular markers monitoring these events to not only assess acute cytotoxicity but to address, as comprehensively as possible, deregulations of physiological signalling processes. To identify MIEs, analysis at the single cell level in real time might be superior to bulk analysis and needs to be established and assessed in the coming years, bearing in mind the enhanced sensitivity of single cells relative to confluent cell monolayers, as demonstrated in Figure S2.

Employment of in vitro studies including HT/C assays has been validated to predict acute toxicity of chemicals in humans (Schoonen et al. 2013). Genotoxicity of chemicals can also be reliably assessed by HT/C methods, by the use of reporter genes under the control of p53 or gadd45a response elements, with similarly accuracy as approved regulatory

tests such as the micronucleus assay (Westerink et al. 2013). Building on this experience, more refined assays focusing on increasingly sophisticated toxicity read-outs, such as inflammation, genotoxicity or disturbance of differentiation and development, should be included in a HT/C screening format to broaden the applicability and relevance of current in vitro screening approaches for testing MNMs.

In conclusion, employment of HT/C assays allows hazard ranking of numerous MNMs under standardised conditions across many cell types. Inspired by the OECD list of representative MNMs, silver, titanium dioxide, cerium oxide, zinc oxide and silicon dioxide were assessed for toxicity using multiple endpoints. A major finding of our concerted studies is the clear cell type-specific action of several MNMs. Whereas Ag and ZnO MNMs are toxic in all cell types, SiO<sub>2</sub> MNMs dependent on surface functionalization appear selectively hazardous to macrophages. Moreover, TiO<sub>2</sub> MNMs affect liver and colon cells by inducing apoptosis. Importantly, ranking of different MNMs by HT/C assays critically depends on the deposited dose, which in addition to the nominal dose, needs to be considered and calculated by appropriate computational methods.

**Acknowledgements** The authors acknowledge support from the European Commission's 7th Framework Programme project NanoMILE (Contract No. NMP4-LA-2013-310451).

#### Compliance with ethical standards

**Conflict of interest** The authors declare that they have no conflict of interest.

**Ethical approval** This article does not contain any studies with human participants or animals performed by any of the authors.

## References

- Al-Rawi M, Diabaté S, Weiss C (2011) Uptake and intracellular localization of submicron and nano-sized SiO<sub>2</sub> particles in HeLa cells. *Arch Toxicol* 85:813–826
- Anguissola S, Garry D, Salvati A, O'Brien PJ, Dawson KA (2014) High content analysis provides mechanistic insights on the pathways of toxicity induced by amine-modified polystyrene nanoparticles. *PLoS One* 9:e108025
- Armand L, Tarantini A, Beal D, Biola-Clier M, Bobyk L, Sorieul S, Pernet-Gallay K, Marie-Desvergne C, Lynch I, Herlin-Boime N, Carriere M (2016) Long-term exposure of A549 cells to titanium dioxide nanoparticles induces DNA damage and sensitizes cells towards genotoxic agents. *Nanotoxicology* 10:913–923
- Cerec V, Glaise D, Garnier D, Morosan S, Turlin B, Drenou B, Gripon P, Kremsdorf D, Guguen-Guillouzo C, Corlu A (2007) Transdifferentiation of hepatocyte-like cells from the human hepatoma HepaRG cell line through bipotent progenitor. *Hepatology* 45:957–967
- Cho WS, Duffin R, Howie SE, Scotton CJ, Wallace WA, MacNee W, Bradley M, Megson IL, Donaldson K (2011) Progressive severe

- lung injury by zinc oxide nanoparticles; the role of Zn<sup>2+</sup> dissolution inside lysosomes. *Part Fibre Toxicol* 8:27
- de Vandebriel RJ, Jong WH (2012) A review of mammalian toxicity of ZnO nanoparticles. *Nanotechnol Sci Appl* 5:61–71
- Delaval M, Wohlleben W, Landsiedel R, Baeza-Squiban A, Boland S (2017) Assessment of the oxidative potential of nanoparticles by the cytochrome c assay: assay improvement and development of a high-throughput method to predict the toxicity of nanoparticles. *Arch Toxicol* 91:163–177
- DeLoid G, Cohen JM, Darrah T, Derk R, Rojasasakul L, Pyrgiotakis G, Wohlleben W, Demokritou P (2014) Estimating the effective density of engineered nanomaterials for in vitro dosimetry. *Nat Commun* 5:3514
- DeLoid GM, Cohen JM, Pyrgiotakis G, Pirela SV, Pal A, Liu J, Srebric J, Demokritou P (2015) Advanced computational modeling for in vitro nanomaterial dosimetry. *Part Fibre Toxicol* 12:32
- DeLoid GM, Cohen JM, Pyrgiotakis G, Demokritou P (2017) Preparation, characterization, and in vitro dosimetry of dispersed, engineered nanomaterials. *Nat Protoc* 12:355–371
- Deschamps E, Weidler PG, Friedrich F, Weiss C, Diabaté S (2014) Characterization of indoor dust from Brazil and evaluation of the cytotoxicity in A549 lung cells. *Environ Geochem Health* 36:225–233
- Dilger M, Orasche J, Zimmermann R, Paur HR, Diabaté S, Weiss C (2016) Toxicity of wood smoke particles in human A549 lung epithelial cells: the role of PAHs, soot and zinc. *Arch Toxicol* 90:3029–3044
- Donauer J, Schreck I, Liebel U, Weiss C (2012) Role and interaction of p53, BAX and the stress-activated protein kinases p38 and JNK in benzo(a)pyrene-diolepoxide induced apoptosis in human colon carcinoma cells. *Arch Toxicol* 86:329–337
- ECHA (2016) Proposal for harmonised classification and labelling. Substance name: Titanium dioxide. European Chemicals Agency. <https://echa.europa.eu/documents/10162/594bf0e6-8789-4499-b9ba-59752f4eafab>. Accessed 7 Nov 2017
- Efeyan A, Serrano M (2007) p53: guardian of the genome and policeman of the oncogenes. *Cell Cycle* 6:1006–1010
- European commission (2013) Examination and assessment of consequences for industry, consumers, human health and the environment of possible options for changing the REACH requirements for nanomaterials. Final report. [http://ec.europa.eu/environment/chemicals/nanotech/pdf/Final\\_Report.pdf](http://ec.europa.eu/environment/chemicals/nanotech/pdf/Final_Report.pdf). Joint Research Centre, Institute for Health and Consumer Protection, Reference: IHCP/2011/I/05/27/OC. Accessed 7 Nov 2017
- Gebel T, Foth H, Damm G, Freyberger A, Kramer PJ, Liliensblum W, Röhl C, Schupp T, Weiss C, Wollin KM, Hengstler JG (2014) Manufactured nanomaterials: categorization and approaches to hazard assessment. *Arch Toxicol* 88:2191–2211
- Gerloff K, Landesmann B, Worth A, Munn S, Palosaari T, Whelan M (2017) The adverse outcome pathway approach in nanotoxicology. *Comput Toxicol* 1:3–11
- Godoy P, Hewitt NJ, Albrecht U, Andersen ME, Ansari N, Bhattacharya S, Bode JG, Bolleyn J, Borner C, Bottger J, Braeuning A, Budinsky RA, Burkhardt B, Cameron NR, Camussi G, Cho CS, Choi YJ, Craig RJ, Dahmen U, Damm G, Dirsch O, Donato MT, Dong J, Dooley S, Drasdo D, Eakins R, Ferreira KS, Fonsato V, Fraczek J, Gebhardt R, Gibson A, Glanemann M, Goldring CE, Gomez-Lechon MJ, Groothuis GM, Gustavsson L, Guyot C, Hallifax D, Hammad S, Hayward A, Haussinger D, Hellerbrand C, Hewitt P, Hoehme S, Holzhutter HG, Houston JB, Hrach J, Ito K, Jaeschke H, Keitel V, Kelm JM, Kevin PB, Kordes C, Kullak-Ublick GA, LeCluyse EL, Lu P, Luebke-Wheeler J, Lutz A, Maltman DJ, Matz-Soja M, McMullen P, Merfort I, Messner S, Meyer C, Mwinyi J, Naisbitt DJ, Nussler AK, Olinga P, Pampaloni F, Pi J, Pluta L, Przyborski SA, Ramachandran A, Rogiers V, Rowe C, Schelcher C, Schmich K, Schwarz M, Singh B, Stelzer EH, Stieger B, Stober R, Sugiyama Y, Tetta C, Thasler WE, Vanhaecke T, Vinken M, Weiss TS, Widera A, Woods CG, Xu JJ, Yarborough KM, Hengstler JG (2013) Recent advances in 2D and 3D in vitro systems using primary hepatocytes, alternative hepatocyte sources and non-parenchymal liver cells and their use in investigating mechanisms of hepatotoxicity, cell signaling and ADME. *Arch Toxicol* 87:1315–1530
- Gordon T, Fine JM (1993) Metal fume fever. *Occup Med* 8:504–517
- Hoppstädter J, Seif M, Dembek A, Cavalius C, Huwer H, Kraegeloh A, Kiemer AK (2015) M2 polarization enhances silica nanoparticle uptake by macrophages. *Front Pharmacol* 6:55
- Horvat T, Landesmann B, Lostia A, Vinken M, Munn S, Whelan M (2017) Adverse outcome pathway development from protein alkylation to liver fibrosis. *Arch Toxicol* 91:1523–1543
- Hussain S, Thomassen LCJ, Ferecatu I, Borot MC, Andreau K, Martens JA, Fleury J, Baeza-Squiban A, Marano F, Boland S (2010) Carbon black and titanium dioxide nanoparticles elicit distinct apoptotic pathways in bronchial epithelial cells. *Part Fibre Toxicol* 7:10
- Jensen KA, Kembouche Y, Christiansen E, Jacobsen NR, Wallin H, Guiot C, Spalla O, Witschger O (2011) Final protocol for producing suitable manufactured nanomaterial exposure media—standard operation procedure (SPO) and background documentation. NanoGenoTox report. [https://www.anses.fr/en/system/files/nanogenotox\\_deliverable\\_5.pdf](https://www.anses.fr/en/system/files/nanogenotox_deliverable_5.pdf). Accessed 7 Nov 2017
- Jensen-Waern M, Melin L, Lindberg R, Johannisson A, Petersson L, Wallgren P (1998) Dietary zinc oxide in weaned pigs—effects on performance, tissue concentrations, morphology, neutrophil functions and faecal microflora. *Res Vet Sci* 64:225–231
- Johnston HJ, Hutchison GR, Christensen FM, Peters S, Hankin S, Stone V (2009) Identification of the mechanisms that drive the toxicity of TiO<sub>2</sub> particulates: the contribution of physicochemical characteristics. *Part Fibre Toxicol* 6:33
- Johnston HJ, Hutchison G, Christensen FM, Peters S, Hankin S, Stone V (2010) A review of the in vivo and in vitro toxicity of silver and gold particulates: particle attributes and biological mechanisms responsible for the observed toxicity. *Crit Rev Toxicol* 40:328–346
- Jones SW, Roberts RA, Robbins GR, Perry JL, Kai MP, Chen K, Bo T, Napier ME, Ting JP, DeSimone JM, Bear JE (2013) Nanoparticle clearance is governed by Th1/Th2 immunity and strain background. *J Clin Invest* 123:3061–3073
- Jovanovic B (2015) Critical review of public health regulations of titanium dioxide, a human food additive. *Integr Environ Assess Manag* 11:10–20
- Kanebratt KP, Andersson TB (2008) Evaluation of HepaRG cells as an in vitro model for human drug metabolism studies. *Drug Metab Dispos* 36:1444–1452
- Keller J, Wohlleben W, Ma-Hock L, Strauss V, Gröters S, Küttler K, Wiench K, Herden C, Oberdörster G, Van RB, Landsiedel R (2014) Time course of lung retention and toxicity of inhaled particles: short-term exposure to nano-Ceria. *Arch Toxicol* 88:2033–2059
- Kim KT, Tanguay RL (2014) The role of chorion on toxicity of silver nanoparticles in the embryonic zebrafish assay. *Environ Health Toxicol* 29:e2014021
- Klein CL, Comero S, Stahlmecke B, Romazanov J, Kuhlbusch TAJ, Van Doren E, De Temmerman P-J, Mast J, Wick P, Krug H, Locoro G, Hund-Rinke K, Kördel W, Friedrichs S, Maier G, Werner J, Linsinger T, Gawlik BM (2011) NM-300 silver. Characterisation, stability, homogeneity. Publications Office of the European Union, European Union
- Kroemer G, Galluzzi L, Brenner C (2007) Mitochondrial membrane permeabilization in cell death. *Physiol Rev* 87:99–163
- Landesmann B (2015) Protein alkylation leading to liver fibrosis. aop wiki. <https://aopwiki.org/wiki/images/c/c0/Aop38-Snapshot-March2015.pdf>. Accessed 7 Nov 2017

- Landesmann B, Goumenou M, Munn S, Whelan M (2012) Description of prototype modes-of-action related to repeated dose toxicity. Publications Office of the European Union, European Union
- Lester E, Blood P, Denyer J, Giddings D, Azzopardi B, Poliakoff M (2006) Reaction engineering: the supercritical water hydrothermal synthesis of nano-particles. *J Supercrit Fluid* 37:209–214
- Lester E, Tang SVY, Khloubystov A, Loczenski Rose V, BATTERY L, Roberts CJ (2013) Producing nanotubes of biocompatible hydroxyapatite by continuous hydrothermal synthesis. *Cryst Eng Comm* 15:3256
- Ling XB (2008) High throughput screening informatics. *Comb Chem High Throughput Screen* 11:249–257
- Liu R, Hassan T, Rallo R, Cohen Y (2013) HDAT: web-based high-throughput screening data analysis tools. *Comput Sci Disc* 6:014006
- Lynch I, Weiss C, Valsami-Jones E (2014) A strategy for grouping of nanomaterials based on key physico-chemical descriptors as a basis for safer-by-design NMs. *Nano Today* 9:266–270
- Marquardt C, Fritsch-Decker S, Al-Rawi M, Diabaté S, Weiss C (2017) Autophagy induced by silica nanoparticles protects RAW264.7 macrophages from cell death. *Toxicology* 379:40–47
- Menendez D, Inga A, Resnick MA (2009) The expanding universe of p53 targets. *Nat Rev Cancer* 9:724–737
- Mennecozzi M, Landesmann B, Harris GA, Liska R, Whelan M (2012) Hepatotoxicity screening taking a mode-of-action approach using HepaRG cells and HCA. *ALTEX Proc WC8* 1:193–204
- Morishige T, Yoshioka Y, Inakura H, Tanabe A, Narimatsu S, Yao X, Monobe Y, Imazawa T, Tsunoda S, Tsutsumi Y, Mukai Y, Okada N, Nakagawa S (2012) Suppression of nanosilica particle-induced inflammation by surface modification of the particles. *Arch Toxicol* 86:1297–1307
- Mühlhopt S, Diabaté S, Krebs T, Weiss C, Paur HR (2009) Lung toxicity determination by in vitro exposure at the air-liquid interface with an integrated online dose measurement. *J Phys* 170:012008
- Nel A, Xia T, Meng H, Wang X, Lin S, Ji Z, Zhang H (2013) Nanomaterial toxicity testing in the 21st century: use of a predictive toxicological approach and high-throughput screening. *Acc Chem Res* 46:607–621
- OECD (2010) Series on the safety of manufactured nanomaterials No. 27. List of manufactured nanomaterials and list of endpoints for phase one of the sponsorship programme for the testing of manufactured nanomaterials: revision. Organization for Economic Co-operation and Development (OECD), Environment directorate, Paris
- Ojea-Jimenez I, Urban P, Barahona F, Pedroni M, Capomaccio R, Ceccone G, Kinsner-Ovaskainen A, Rossi F, Gilliland D (2016) Highly flexible platform for tuning surface properties of silica nanoparticles and monitoring their biological interaction. *ACS Appl Mater Interfaces* 8:4838–4850
- Panas A, Marquardt C, Nalcaci O, Bockhorn H, Baumann W, Paur HR, Mühlhopt S, Diabaté S, Weiss C (2013) Screening of different metal oxide nanoparticles reveals selective toxicity and inflammatory potential of silica nanoparticles in lung epithelial cells and macrophages. *Nanotoxicology* 7:259–273
- Panas A, Comouth A, Saathoff H, Leisner T, Al-Rawi M, Simon M, Seemann G, Dössel O, Mühlhopt S, Paur HR, Fritsch-Decker S, Weiss C, Diabaté S (2014) Silica nanoparticles are less toxic to human lung cells when deposited at the air-liquid interface compared to conventional submerged exposure. *Beilstein J Nanotechnol* 5:1590–1602
- Park EJ, Yi J, Chung KH, Ryu DY, Choi J, Park K (2008) Oxidative stress and apoptosis induced by titanium dioxide nanoparticles in cultured BEAS-2B cells. *Toxicol Lett* 180:222–229
- Pele LC, Thoree V, Bruggraber SF, Koller D, Thompson RP, Lomer MC, Powell JJ (2015) Pharmaceutical/food grade titanium dioxide particles are absorbed into the bloodstream of human volunteers. *Part Fibre Toxicol* 12:26
- Piret JP, Bondarenko OM, Boyles MSP, Himly M, Ribeiro AR, Benetti F, Smal C, Lima B, Potthoff A, Simion M, Dumortier E, Leite PEC, Balottin LB, Granjeiro JM, Ivask A, Kahru A, Radauer-Preiml I, Tischler U, Duschl A, Saout C, Anguissola S, Haase A, Jacobs A, Nelissen I, Misra SK, Toussaint O (2017) Pan-European inter-laboratory studies on a panel of in vitro cytotoxicity and pro-inflammation assays for nanoparticles. *Arch Toxicol* 91:2315–2330
- Ramuz O, Isnardon D, Devilard E, Charafe-Jauffret E, Hassoun J, Birg F, Xerri L (2003) Constitutive nuclear localization and initial cytoplasmic apoptotic activation of endogenous caspase-3 evidenced by confocal microscopy. *Int J Exp Pathol* 84:75–81
- Rasmussen K, Mast J, De Temmerman PJ, Verleysen E, Waegeneers N, Van Steen F, Pizzolon JC, De Temmerman L, Van Doren E, Jensen KA, Birkedal R, Levin M, Nielsen SH, Koponen IK, Clausen PA, Kofeod-Sorensen V, Kembouche Y, Thieriet N, Spalla O, Guiot C, Rousset D, Witschger O, Bau S, Bianchi B, Motzkus C, Shivachev B, Dimova L, Nikolova R, Nihtianova D, Tarassov M, Petrov O, Bakardjieva S, Gilliland D, Pianella F, Ceccone G, Spampinato V, Cotogno G, Gibson N, Gaillard C, Mech A (2014) Titanium dioxide, NM-100, NM-101, NM-102, NM-103, NM-104, NM-105: characterisation and physico-chemical properties. Publications Office of the European Union, European Union
- Reidy B, Haase A, Luch A, Dawson KA, Lynch I (2013) Mechanisms of silver nanoparticle release, transformation and toxicity: a critical review of current knowledge and recommendations for future studies and applications. *Materials* 6:2295–2350
- Röttgermann PJ, Alberola AP, Rädler JO (2014a) Cellular self-organization on micro-structured surfaces. *Soft Matter* 10:2397–2404
- Röttgermann PJ, Hertrich S, Berts I, Albert M, Segerer FJ, Moulin JF, Nickel B, Rädler JO (2014b) Cell motility on polyethylene glycol block copolymers correlates to fibronectin surface adsorption. *Macromol Biosci* 14:1755–1763
- Sayes CM, Wahi R, Kurian PA, Liu Y, West JL, Ausman KD, Warheit DB, Colvin VL (2006) Correlating nanoscale titania structure with toxicity: a cytotoxicity and inflammatory response study with human dermal fibroblasts and human lung epithelial cells. *Toxicol Sci* 92:174–185
- Schoonen WGEJ, Westerink WMA, Van de Water FM, Jean HG (2013) High-throughput toxicity testing in drug development: aim, strategies, and novel trends. In: Steinberg P (ed) High-throughput screening methods in toxicity testing. Wiley, Hoboken, pp 33–75
- Schreck I, Deigendesch U, Burkhardt B, Marko D, Weiss C (2012) The Alternaria mycotoxins alternariol and alternariol methyl ether induce cytochrome P450 1A1 and apoptosis in murine hepatoma cells dependent on the aryl hydrocarbon receptor. *Arch Toxicol* 86:625–632
- Sha B, Gao W, Cui X, Wang L, Xu F (2015) The potential health challenges of TiO<sub>2</sub> nanomaterials. *J Appl Toxicol* 35:1086–1101
- Shi Y, Wang F, He J, Yadav S, Wang H (2010) Titanium dioxide nanoparticles cause apoptosis in BEAS-2B cells through the caspase 8/t-Bid-independent mitochondrial pathway. *Toxicol Lett* 196:21–27
- Shi H, Magaye R, Castranova V, Zhao J (2013) Titanium dioxide nanoparticles: a review of current toxicological data. *Part Fibre Toxicol* 10:15
- Singh C, Friedrichs S, Levin M, Birkedal R, Jensen KA, Pojana G, Wohlleben W, Schulte S, Wiench K, Turney T, Koulaeva O, Marshall D, Hund-Rinke K, Kördel W, Van Doren E, De Temmerman PJ, Abi Daoud Francisco M, Mast J, Gibson N, Koeber R, Linsinger T, Klein CL (2011) Zinc oxide NM-110, NM-111, NM-112, NM-113. Characterisation and test item preparation. Publications Office of the European Union, European Union



- Singh C, Friedrichs S, Ceccone G, Gibson N, Jensen KA, Levin M, Infante HG, Carlander D, Rasmussen K (2014) Cerium dioxide, NM-211, NM-212, NM-213. Characterisation and test item preparation. Publications Office of the European Union, European Union
- Stern ST, Adiseshaiah PP, Christ RM (2012) Autophagy and lysosomal dysfunction as emerging mechanisms of nanomaterial toxicity. *Part Fibre Toxicol* 9:20
- Tralau T, Oelgeschlager M, Gurtler R, Heinemeyer G, Herzler M, Hofer T, Itter H, Kuhl T, Lange N, Lorenz N, Muller-Graf C, Pabel U, Pirow R, Ritz V, Schafft H, Schneider H, Schulz T, Schumacher D, Zellmer S, Fleur-Bol G, Greiner M, Lahrssen-Wiederholt M, Lampen A, Luch A, Schonfelder G, Solecki R, Wittkowski R, Hensel A (2015) Regulatory toxicology in the twenty-first century: challenges, perspectives and possible solutions. *Arch Toxicol* 89:823–850
- Valko M, Rhodes CJ, Moncol J, Izakovic M, Mazur M (2006) Free radicals, metals and antioxidants in oxidative stress-induced cancer. *Chem Biol Interact* 160:1–40
- Wang F, Bexiga MG, Anguissola S, Boya P, Simpson JC, Salvati A, Dawson KA (2013a) Time resolved study of cell death mechanisms induced by amine-modified polystyrene nanoparticles. *Nanoscale* 5:10868–10876
- Wang F, Yu L, Monopoli MP, Sandin P, Mahon E, Salvati A, Dawson KA (2013b) The biomolecular corona is retained during nanoparticle uptake and protects the cells from the damage induced by cationic nanoparticles until degraded in the lysosomes. *Nanomedicine* 9:1159–1168
- Weir A, Westerhoff P, Fabricius L, Hristovski K, von Goetz N (2012) Titanium dioxide nanoparticles in food and personal care products. *Environ Sci Technol* 46:2242–2250
- Westerink WMA, Stevenson JCR, Horbach GJ, Van de Water FM, Van de Waart B, Schoonen WGEJ (2013) Genotoxicity and carcinogenicity: regulatory and novel test methods. In: Steinberg P (ed) *High-throughput screening methods in toxicity testing*. Wiley, Hoboken, pp 233–269
- Wu W, Bromberg PA, Samet JM (2013) Zinc ions as effectors of environmental oxidative lung injury. *Free Radic Biol Med* 65:57–69
- Xia T, Kovoichich M, Liang M, Zink JJ, Nel AE (2008) Cationic polystyrene nanosphere toxicity depends on cell-specific endocytic and mitochondrial injury pathways. *ACS Nano* 2:85–96
- Yamashita K, Yoshioka Y, Higashisaka K, Mimura K, Morishita Y, Nozaki M, Yoshida T, Ogura T, Nabeshi H, Nagano K, Abe Y, Kamada H, Monobe Y, Imazawa T, Aoshima H, Shishido K, Kawai Y, Mayumi T, Tsunoda S, Itoh N, Yoshikawa T, Yanagihara I, Saito S, Tsutsumi Y (2011) Silica and titanium dioxide nanoparticles cause pregnancy complications in mice. *Nat Nanotechnol* 6:321–328
- Yoon HJ, Cha BS (2014) Pathogenesis and therapeutic approaches for non-alcoholic fatty liver disease. *World J Hepatol* 6:800–811
- Yu F, Chen Z, Wang B, Jin Z, Hou Y, Ma S, Liu X (2016) The role of lysosome in cell death regulation. *Tumour Biol* 37:1427–1436
- Zhao Y, Howe JL, Yu Z, Leong DT, Chu JJ, Loo JS, Ng KW (2013) Exposure to titanium dioxide nanoparticles induces autophagy in primary human keratinocytes. *Small* 9:387–392